Peculiarities of excited state structure and photoluminescence in Bi^{3+}-doped $Lu_3Al_5O_{12}$ single-crystalline films

2009 J. Phys.: Condens. Matter 21 415502

(http://iopscience.iop.org/0953-8984/21/41/415502)

J. Phys.: Condens. Matter **21** (2009) 415502 (9pp) doi:10.1088/0953-8984/21/41/415502

Peculiarities of excited state structure and photoluminescence in Bi^{3+}-doped $Lu_3Al_5O_{12}$ single-crystalline films

V Babin[1], V Gorbenko[2], A Krasnikov[1], A Makhov[1], M Nikl[3], K Polak[3], S Zazubovich[1] and Yu Zorenko[2]

[1] Institute of Physics, University of Tartu, Riia 142, 51014 Tartu, Estonia
[2] Ivan Franko National University of Lviv, 107 General Tarnavsky Street, 79017 Lviv, Ukraine
[3] Institute of Physics ASCR, Cukrovarnicka 10, 162 53 Prague, Czech Republic

E-mail: svet@fi.tartu.ee (S Zazubovich)

Received 14 June 2009, in final form 2 September 2009
Published 23 September 2009
Online at stacks.iop.org/JPhysCM/21/415502

Abstract

Single-crystalline films of $Lu_3Al_5O_{12}$:Bi, prepared by the liquid phase epitaxy method from the melt-solution based on Bi_2O_3 flux, have been studied at 4.2–400 K by time-resolved luminescence spectroscopy methods. Their emission spectra consist of two types of bands with strongly different characteristics. The ultraviolet emission band consists of two components, arising from the electronic transitions which correspond to the $^3P_1 \rightarrow {}^1S_0$ and $^3P_0 \rightarrow {}^1S_0$ transitions in a free Bi^{3+} ion. At low temperatures, mainly the lower-energy component of this emission is observed, having the decay time $\sim 10^{-3}$ s at $T < 100$ K and arising from the metastable $^3P_0$ level. At $T > 100$ K, the higher-energy emission component appears, arising from the thermally populated emitting $^3P_1$ level. The visible emission spectrum consists of two dominant strongly overlapped broad bands with large Stokes shifts. At 4.2 K, their decay times are $\sim 10^{-5}$ s and decrease with increasing temperature. Both of the visible emission bands are assumed to have an exciton origin. The lower-energy band is ascribed to an exciton, localized near a single Bi^{3+} ion. The higher-energy band shows a stronger intensity dependence on the Bi^{3+} content and is assumed to arise from an exciton localized near a dimer Bi^{3+} center. The origin and structure of the corresponding excited states is considered and the processes, taking place in the excited states, are discussed.

(Some figures in this article are in colour only in the electronic version)

1. Introduction

Bi^{3+} centers in different materials (alkali halides, alkaline-earth oxides, sulfates and phosphates, rare-earth oxide-based materials, etc) have been studied for more than 45 years (see, e.g., [1–18] and references therein). The Bi^{3+}-doped rare-earth aluminate and gallate garnets, where a Bi^{3+} ion substitutes a trivalent rare-earth ion, can be considered as prospective materials for scintillators due to an intense and fast Bi^{3+}-related luminescence [14, 16, 17]. However, optical characteristics of Bi^{3+}-doped garnets have been studied only in a few papers [3, 11, 14–17]. In the emission spectrum of $Y_3Ga_5O_{12}$:Bi [14, 15], $Gd_3Ga_5O_{12}$:Bi [15], $Y_3Al_5O_{12}$:Bi [15–17] and $Lu_3Al_5O_{12}$:Bi [15, 17], two main emission bands were observed, located in the ultraviolet and visible spectral ranges. The characteristics of the ultraviolet emission are very similar to those in CaO:Bi crystals (see, e.g., [4, 5, 13] and references therein). This emission was ascribed to the radiative decay of the triplet relaxed excited state of Bi^{3+} centers [14, 15]. It consists of two components, arising from the electronic transitions, corresponding to the $^3P_1 \rightarrow {}^1S_0$ and $^3P_0 \rightarrow {}^1S_0$ transitions in a free Bi^{3+} ion [14]. The origin of the visible emission is still not clear. It was ascribed to the Bi^{3+}-related bound exciton [11] or to pairs and/or clusters of Bi^{3+} ions [15–17].

In single-crystalline films of $Y_3Al_5O_{12}$:Bi and $Lu_3Al_5O_{12}$:Bi, prepared by the liquid phase epitaxy method, a large and variable concentration of Bi^{3+} ions can be achieved [16, 17].

Table 1. The maxima positions (E_{max}) and half-widths (FWHM) of the emission bands, excitation band maxima (E_{exc}) and Stokes shifts (S) at 80 K as well as luminescence decay times (τ) at 4.2 K obtained for the UV and vis emission bands of Bi^{3+}-related centers in LuAG:Bi.

E_{max} (eV)	FWHM (eV)	E_{exc} (eV)	S (eV)	τ	E_{max} (eV) in uncorrected time-resolved spectra at 4.2 K
4.08	0.24	∼5.95; 4.63	0.55	1100 μs	4.05
4.19	0.27	∼5.95; 4.63	0.44	0.1–0.4 ns	
2.60	0.87	∼5.95; 4.60	2.00	26 μs; 72 μs	2.79
2.75	0.90	5.20; ∼4.40	1.60	40 μs	2.93

The aim of this work was to investigate the luminescence characteristics of $Lu_3Al_5O_{12}$:Bi single-crystalline films, to obtain information on the origin and structure of the corresponding excited states, and to clarify the processes taking place in the excited states.

2. Experimental details

Single-crystalline films (SCF) of $Lu_3Al_5O_{12}$:Bi (LuAG:Bi) with a thickness, varying from 8 to 12 μm, were grown by the liquid phase epitaxy (LPE) method from the melt solution, based on a Bi_2O_3 oxide flux [17]. Single crystals of $Y_3Al_5O_{12}$ (YAG) were used as substrates. The concentration of Bi^{3+} ions in the SCF was determined with a JEOL JXA-733 electron microprobe analyzer. Three samples with different Bi^{3+} concentrations (1.34, 0.183 and 0.07 at.%) were investigated. For comparison, the luminescence characteristics of the YAG substrate were also studied at the same conditions.

The steady-state emission and excitation spectra and temperature dependences of the emission intensity were measured in the 80–330 K temperature range under selective excitation in the 2.4–6.2 eV energy range at a set-up consisting of a deuterium DDS-400 lamp, two monochromators (SF-4 and SPM-1) and a photomultiplier (FEU-39 or FEU-79) with an amplifier and recorder. The spectra were corrected for the spectral distribution of the excitation light, the transmission and dispersion of the monochromators and the spectral sensitivity of the detectors.

Luminescence decay kinetics in the μs–ms time range were measured at 4.2–300 K at the same set-up but under excitation with a xenon flash lamp FX-1152 (EG&G) (a pulse duration of about 1 μs and maximum repetition frequency of 300 Hz). The decay curves $I(t)$ were measured at the same conditions for different emission and excitation energies. This allows one to obtain time-resolved emission and excitation spectra at any moment of time (t) after the excitation pulse. The $I(t)$ curves in the ns time range were measured at 10–300 K under synchrotron excitation at the SUPERLUMI station (HASYLAB at DESY, Hamburg, Germany). At 80–400 K, the decay kinetics was measured with a modified Spectrofluorometer 199S (Edinburgh Instruments) under excitation with a nanosecond coaxial hydrogen-filled flashlamp or microsecond Xe lamp (both IBH Scotland) and using two single grating monochromators. The detection was performed with a IBH-04 photomultiplier module using the method of time-correlated single-photon counting. A deconvolution procedure (SpectraSolve software package) was applied to extract true decay times using the multiexponential approximation. The experiments at low temperatures were carried out with the use of an immersion helium cryostat or vacuum nitrogen cryostat.

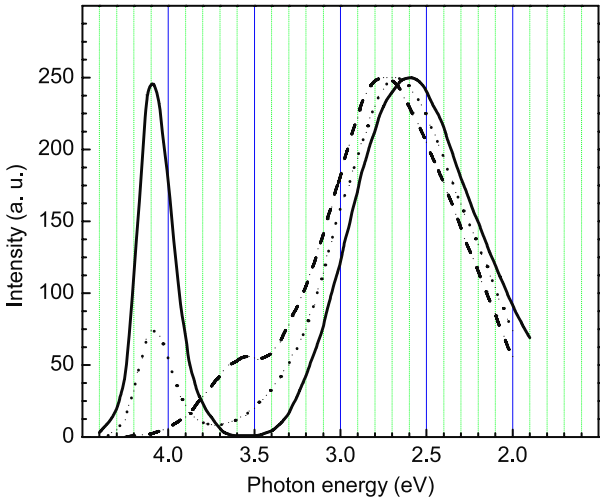

Figure 1. Emission spectra (normalized) of LuAG:Bi SCF measured at 80 K under 4.6 eV (solid line), 5.3 eV (dashed line) and 4.35 eV (dotted line) excitations.

3. Experimental results

The absorption spectra of the LuAG:Bi samples studied have been reported in [17]. Their emission spectrum is similar to that obtained for many other Bi^{3+}-doped and Bi^{3+}-containing oxide compounds (see, e.g., [7–11, 14–16] and references therein). In the emission spectrum, two types of bands with strongly different characteristics are observed. The complex ultraviolet (UV) band is located around 4.1 eV and the complex visible (vis) band around 2.7 eV (figure 1). The characteristics of separate components of the UV and vis bands are independent of the Bi^{3+} content and are similar in all the SCF studied. They are summarized in table 1. Both the UV and vis bands surely arise from the presence of Bi^{3+} ions in the SCF.

3.1. Characteristics of the UV luminescence

At $T < 100$ K, the main UV emission band is located at 4.08 eV (FWHM = 0.24 eV) (figure 2, solid line). In the excitation spectrum of this emission, wide bands around 5.95 and 4.63 eV are observed (figure 3, solid line). Their shape is distorted due to a very large optical density (OD > 4).

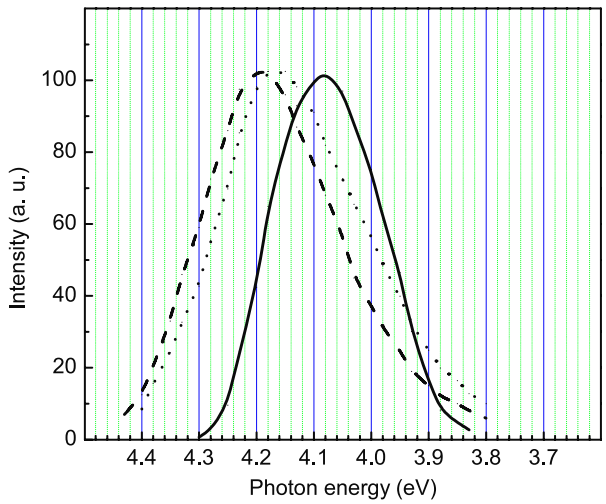

Figure 2. Ultraviolet emission spectra (normalized) of LuAG:Bi SCF measured at 80 K (solid line), 150 K (dashed line) and 300 K (dotted line). $E_{exc} = 4.6$ eV.

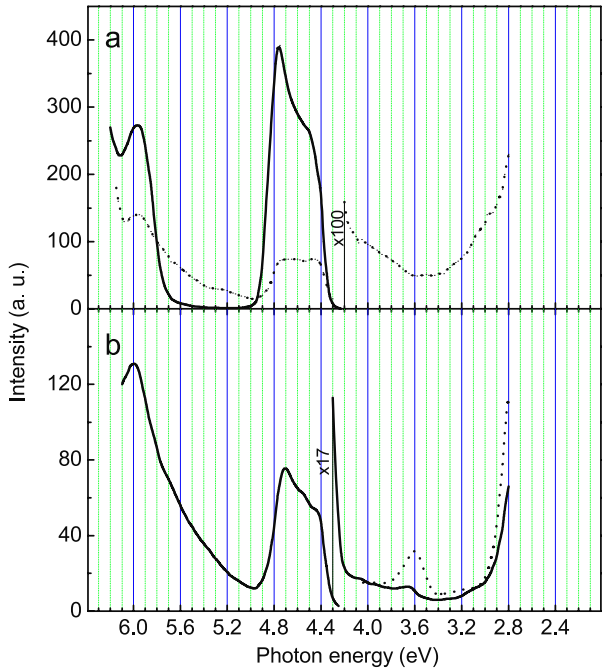

Figure 3. (a) Excitation spectra (normalized) of the ultraviolet (solid line) and visible (dotted line) emissions of LuAG:Bi SCF. (b) The comparison of the excitation spectra of the 2.4 eV (Ce^{3+}) emission of LuAG:Bi SCF (solid line) and LuAG:Ce single crystal (dotted line). $T = 80$ K.

The Stokes shift is 0.55 eV. Under excitation in the 5.1–5.3 eV energy range, the intensity of the 4.08 eV emission is negligible. As the temperature increases up to 150 K, the maximum of the UV emission band is shifted up to 4.19 eV (FWHM = 0.27 eV) (figure 2, dashed line). These data indicate the presence of two components in the UV emission spectrum. The 4.19 eV emission band is the superposition of the 4.08 eV band and the higher-energy emission band arising from the upper energy level. The

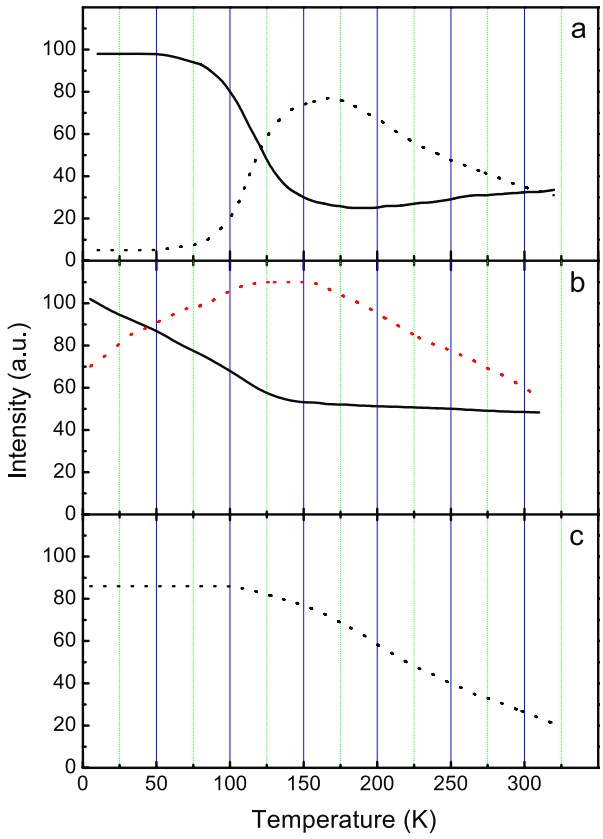

Figure 4. Temperature dependences of the emission intensities measured for: (a) two opposite sides of the ultraviolet emission band at $E_{em} = 3.95$ eV (solid line) and $E_{em} = 4.32$ eV (dotted line) under $E_{exc} = 4.6$ eV; (b) the maximum intensity of the UV emission (solid line) and of the 2.6 eV emission (dotted line) under 4.6 eV excitation; (c) the 2.75 eV emission under 5.1 eV excitation.

thermally stimulated redistribution of their intensities occurs around 115 K (figure 4(a)). The activation energy E_a of this process, calculated from the $\ln I(1/T)$ dependences, is about 85 meV. At $T > 180$ K, the emission band maximum gradually shifts back (to 4.15 eV at 300 K, figure 2, dotted line) which explains the reverse redistribution of the emission intensities shown in figure 4(a). In the temperature range of 4.2–150 K, the intensity of the UV emission decreases about twice and then remains practically constant (figure 4(b)).

In the decay kinetics of the UV emission at 4.2 K, mainly a slow component is observed with the decay time $\tau = 1.1$ ms (figure 5). A very weak fast component is also present with the decay time 0.1–0.4 ns. Its light sum is at least smaller by two orders of magnitude as compared with the light sum of the slow component. The time-resolved emission spectrum of the slow component (see the inset) does not change in time. As the temperature increases, the decay time value remains constant up to about 100 K and then decreases with an activation energy of 84 ± 2 meV, reaching the value of 20 μs at 200 K and $\approx$1 μs at 300 K. A similar temperature dependence of the slow component decay time was observed for the triplet emission of Bi^{3+} centers in some other hosts (see, e.g., [8, 13, 14, 18]).

The temperature dependences of the emission intensity and decay time indicate that, at $T > 100$ K, the upper energy

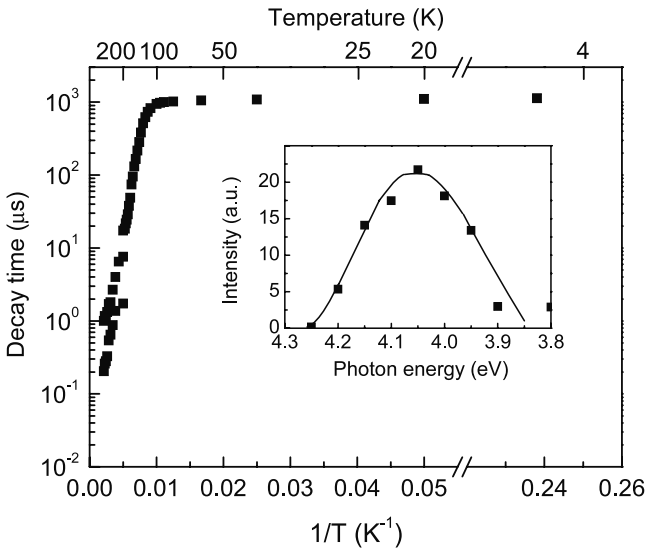

Figure 5. Temperature dependence of the decay time of ultraviolet emission measured under $E_{exc} = 4.6$ eV. In the inset, the uncorrected time-resolved emission spectrum is shown measured at 4.2 K at $t = 1000$ μs.

level of the triplet relaxed excited state (RES) of the Bi^{3+} center is thermally populated from the lower level.

Besides the 4.08 eV emission, additional weaker UV emissions are observed at 80 K. The 3.6 eV emission is excited around 5.3 eV (figure 1, dashed line). The 3.32 eV (FWHM = 0.80 eV) emission is excited around 3.92 and 5.25 eV. The Gd^{3+}-induced emission is observed at 3.95 eV. The above-mentioned additional UV emissions are present also in the substrate.

3.2. Characteristics of the visible luminescence

At 80 K, the main excitation bands of the vis emission are located around 5.95, 5.2 and 4.6 eV (figure 3, dotted line). Under excitation in the 4.4–4.9 eV range and around 5.95 eV, a strong visible emission band is peaking at 2.6 eV (FWHM = 0.87 eV) (figure 1, solid line). Under excitation around 5.2 eV (dashed line) and at 4.35 eV (dotted line), the weaker emission band shifted to higher energies (up to 2.75 eV; FWHM = 0.90 eV) is observed. The temperature dependences of the vis emission intensity measured under 4.6 and 5.2 eV excitations are different (compare dotted lines in figures 4(b) and (c)): the intensities decrease twice around 300 K and 240 K, respectively. Both the 2.6 and 2.75 eV emissions are surely connected with the presence of Bi^{3+} ions in LuAG. However, in the YAG substrate, the 2.68 eV emission (FWHM = 0.90 eV) is observed. This emission is excited mainly at $E_{exc} > 5.1$ eV but also around 4.5 eV. The emission intensity is constant up to 100 K and then decreases twice around 160 K. Therefore, the characteristics of the LuAG:Bi emission can be distorted due to its overlap with the above-mentioned emission band of the substrate.

In the 4.4–4.9 eV energy range, the excitation band of the 2.6 eV emission (figure 3, dotted line) is close to that of the UV emission (solid line). In principle, this effect could be explained by the reabsorption of the UV emission in the absorption band of the vis emission center. As is evident from figure 3 (dotted line), a visible emission of LuAG:Bi is really excited around 3.8–4.2 eV. However, under this excitation, the emission spectrum consists of narrower 2.4 and 2.15 eV bands. Thus, it is strongly different from that observed under excitation in the 4.4–4.9 eV energy range (figure 1). The similarity of the excitation spectra of the UV and 2.6 eV emissions can indicate that both these emissions arise from the same Bi^{3+} center. This assumption is confirmed by the fact that, under 4.6 eV excitation, the decrease of the UV emission intensity (figure 4(b), solid line) is accompanied with the increase of the 2.6 eV emission intensity (dotted line) which takes place with an approximately the same activation energy (6–9 meV). These data indicate the presence of thermally stimulated transitions between the excited states responsible for the UV and the 2.6 eV emission. As the decrease in the UV emission intensity does not result in a shortening of its decay time at $T < 100$ K (figure 5), one can conclude that the excited state, responsible for the 2.6 eV emission, is thermally populated from the nonrelaxed triplet excited of the Bi^{3+} ion.

However, the assumption made above seems to be in disagreement with the conclusion of [15–17] that the vis/UV emission intensity ratio depends on the Bi^{3+} content. Therefore, the emission intensities under excitation around 4.6 eV were compared at the same experimental conditions for three LuAG:Bi SCF samples where the Bi^{3+} content varies by 19 times. It was found that the 2.6 eV emission intensity is practically independent of the Bi^{3+} content. This effect is caused by a huge optical density of the SCF studied (OD > 4 even in the LuAG:0.07 at.% Bi sample). In these SCF, the UV emission intensity should also be independent of the Bi^{3+} content. However, as the Bi^{3+} content increases, the UV emission intensity decreases about 5 times. The above-mentioned decrease can be explained by the (i) increasing reflection of the exciting light; (ii) reabsorption of the UV emission in the 4.63 eV absorption band, resulting in a lower-energy shift of the UV emission band with the increasing Bi^{3+} content (see also [16]) and (iii) aggregation of Bi^{3+} ions, resulting in the formation of Bi^{3+}-related dimers [15–17]; concentration quenching. According to [17], the increase of the vis/UV ratio in the cathodoluminescence spectrum of LuAG:Bi is accompanied with a higher-energy shift of the vis emission band. This can mean that just the higher-energy component of the vis emission has a stronger intensity dependence on the Bi^{3+} content as compared with the 2.6 eV band. This fact allows us to assume that the 2.75 eV band can be connected with dimer Bi^{3+}-related centers.

In the low-temperature decay kinetics of the vis emission, no ns component is observed under any excitation. Under 4.6 ± 0.1 eV excitation, the decay kinetics at 4.2 K is very complicated. The decay curve consists of four components whose decay times are about 26, 72, 228 and 822 μs (see the inset in figure 6(a)). The uncorrected time-resolved emission spectra of the two dominating faster components (measured at different time moments from $t = 16$ to 100 μs) coincide and are located at 2.79 eV (FWHM = 0.78 eV) (figure 7(a), solid line). The excitation spectra of these two decay components

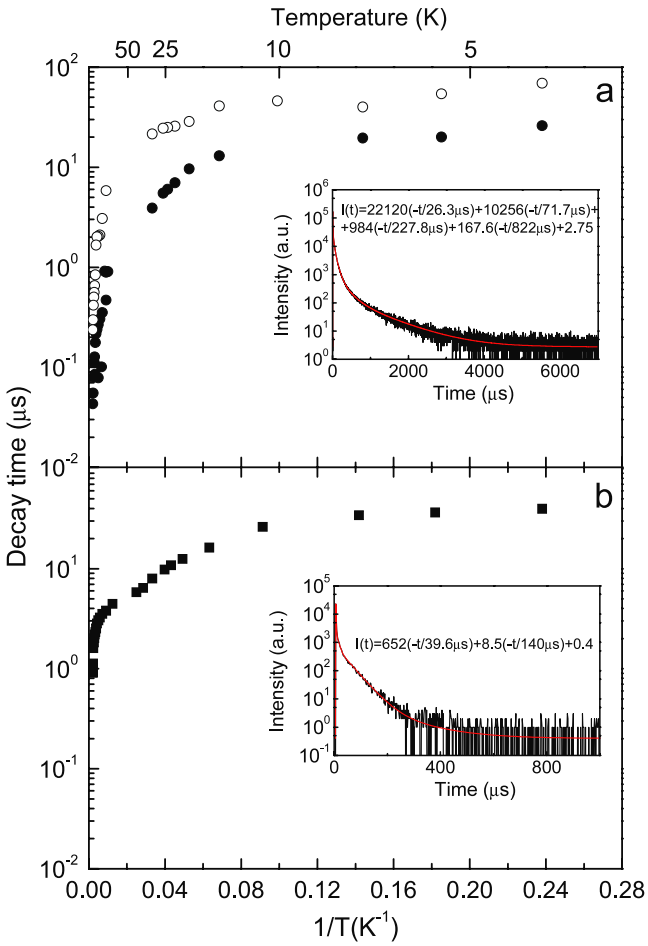

Figure 6. Decay curves at 4.2 K (in the inset) and temperature dependences of the visible emission decay times measured (a) for $E_{em} = 2.4$ eV, $E_{exc} = 4.7$ eV and (b) $E_{em} = 3.2$ eV, $E_{exc} = 5.3$ eV.

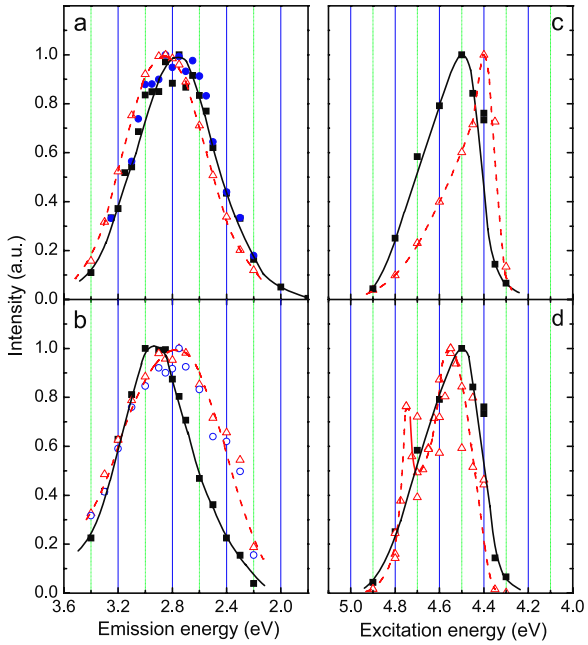

Figure 7. Uncorrected time-resolved emission ((a) and (b)) and excitation ((c) and (d)) spectra measured at 4.2 K. The emission spectra are measured (a) under $E_{exc} = 4.6$ eV at $t = 30$ μs (closed squares) and $t = 100$ μs (closed circles), and under $E_{exc} = 4.35$ eV at $t = 50$ μs (open triangles); (b) under $E_{exc} = 5.2$ eV at $t = 50$ μs (closed squares), $t = 180$ μs (open circles) and $t = 16$ μs (open triangles). The excitation spectra are measured for: (c) $E_{em} = 2.4$ eV at $t = 300$ μs (solid line) and $E_{em} = 3.2$ eV at $t = 30$ μs (dashed line); (d) $E_{em} = 2.4$ eV at $t = 300$ μs (solid line) and $E_{em} = 4.05$ eV at $t = 1000$ μs (dashed line).

coincide as well. This allows us to conclude that the main 26 and 72 μs components arise from the same Bi^{3+}-related emission band. The emission spectra measured at $t > 500$ μs for the two other, much weaker slower decay components are shifted to lower energies and peaking at 2.75 eV (FWHM = 0.74 eV). It means that these components arise from some other emission bands. We assume that the weaker 228 and 822 μs decay components are most probably arising from the above-mentioned 2.68 eV emission of the YAG substrate. The decay times of the two main components start to decrease at $T < 4.2$ K (figure 6(a)). In the temperature range of 4.2–15 K, this process takes place with the activation energy of about 0.19 meV. In the temperature range 25–150 K, the activation energy is about 4.7 ± 0.5 meV. At $T > 150$ K, the further shortening of τ is caused by the thermal quenching of the vis emission (figure 4(b)).

Under 5.3 eV excitation, the decay kinetics of the vis emission at 4.2 K consists of the main component with the decay time of about 40 μs and a much weaker ≈140 μs component (see the inset in figure 6(b)). The latter component can be the superposition of the weak 72 and 228 μs components observed in the decay kinetics of the visible emission under 4.6 eV excitation. The uncorrected time-resolved emission spectrum of the dominating 40 μs component (figure 7(b), solid line) is shifted to higher energies (up to 2.93 eV) and is narrower (FWHM = 0.68 eV) as compared with the emission spectrum of the 26 and 72 μs components dominating under 4.6 eV excitation (figure 7(a), solid line). Thus, one can conclude that the ≈40 μs component arises from the higher-energy vis emission band, and the ≈26 and 72 μs components, from the lower-energy band (table 1). The 40 μs component is excited also around 4.35 eV which reveals itself in the high-energy shift (up to 2.865 eV) and narrowing (FWHM = 0.72 eV) of the time-resolved emission spectrum measured under this excitation (see figure 7(a), dashed line). The emission spectrum of the much weaker 140 μs component as well as the emission spectrum obtained at $t = 16$ μs (figure 7(b), dashed line) are close to the spectra obtained under 4.6 eV excitation (figure 7(a), solid line). These data indicate that the decay components, characteristic for the lower-energy emission, appear also under 5.2 eV excitation, but their light sums are small. It should be noted that, due to the close values of the decay times of the dominating components, there is a strong overlap of the two broad vis emission bands, and their overlap with the emission bands arising from the substrate makes it very difficult to determine the correct values of the decay times. The presented values of τ are calculated with an accuracy of about 10%. The $\tau(T)$ dependence of the fastest component (figure 6(b)) is similar to that observed in figure 6(a). The activation energy at $T < 15$ K is about

0.11 meV and in the 25–100 K range, about 2.7 meV. At higher temperatures, the decrease of τ is caused by the thermal quenching of the emission (figure 4(c)).

The time-resolved excitation spectra measured at 4.2 K for the lower-energy (figure 7(c), solid line) and the higher-energy (dashed line) vis emission are different. The ≈40 μs component, dominating in the decay kinetics of the higher-energy emission, is relatively more effectively excited at the low-energy edge of the 4.6 eV absorption band (at 4.3–4.4 eV) (dashed line). The excitation spectrum of the 72 μs component, arising from the 2.6 eV emission (see, e.g., figures 7(c) and (d), solid lines), is close to that of the UV emission (figure 7(d), dashed line). This conclusion is in agreement with that made above from the study of the steady-state excitation spectra.

Additional weaker visible emission bands are also observed in all the samples studied. The excitation spectra of relatively narrow (FWHM ≈ 0.40–0.45 eV) bands, peaking at 2.40 and 2.15 eV, contain strongly overlapped bands located at 3.9–4.0, 3.5–3.6, 3.3 and 3.05 eV (figure 3(a), dotted line). All the above-mentioned emissions are effectively excited also in the Bi^{3+}-related absorption bands due to the reabsorption of the UV emission of Bi^{3+} centers. However, under $E_{exc} < 4.1$ eV, the additional emission intensities are independent of the Bi^{3+} content. The comparison of the luminescence characteristics of the samples studied with those of the substrate indicates that, besides the above-mentioned 2.68 eV emission, the 2.40 and 2.15 eV emission bands are also observed in the substrate. The Ce^{3+}-related emission bands located at 2.36 and 2.14 eV are also observed in the samples studied. The corresponding excitation bands are located at 2.69 and 3.68 eV (figure 3(b), solid line). Thus, the positions of the Ce^{3+}-related spectral bands are characteristic not for LuAG:Ce (figure 3(b), dotted line) but for YAG:Ce [19]. This indicates that they arise from the contamination of the YAG substrate with Ce^{3+} ions.

4. Discussion

A trivalent Bi^{3+} ion replaces a trivalent Lu^{3+} ion in the eight-coordinated dodecahedral site of the LuAG crystal lattice [20]. Their ionic radii are close (1.17 Å and 0.98 Å, respectively [21]). As, unlike Pb^{2+} centers [22], no charge and volume compensation is needed in this case, a large concentration of single Bi^{3+} centers was achieved in the SCF studied.

According to [23], the energies of electronic transitions from the ground $^1S_0$ level to the excited $^3P_1$, $^3P_2$ and $^1P_1$ levels of a free Bi^{3+} ion (E_{free}) are 9.41 eV, 11.96 eV and 14.21 eV, respectively. In the crystal, the absorption bands, labeled as A, B and C, correspond to the electronic transitions to these levels. The lowest-energy A absorption band of LuAG:Bi, corresponding to the $^1S_0 \rightarrow {}^3P_1$ transition, is located around 4.63 eV, i.e. the transition energy in the crystal (E_{crys}) is about twice as small as compared with that in a free Bi^{3+} ion. Taking into account the fact that the E_{free}/E_{crys} ratio increases with the increasing E_{free} according to the approximate equation $E_{free}/E_{crys} = 1 + kE_{free}$, experimentally found in [24] and confirmed to be valid for all the ns^2-ion-doped alkali halide crystals, the positions of the B and C bands of the Bi^{3+} center in LuAG:Bi can be estimated. One can assume that the ≈5.95 eV band arises from the $^1S_0 \rightarrow {}^1P_1$ transitions. In that case, the B absorption band in LuAG:Bi should be located at about 5.2 eV.

Let us consider the origin and structure of the energy levels responsible for the UV and vis emission bands of a Bi^{3+}-related center in LuAG:Bi.

4.1. Ultraviolet luminescence

The data obtained in the luminescence study clearly indicate that the UV emission of LuAG:Bi arises from the triplet RES of the Bi^{3+} center. The low-temperature emission band, located at 4.08 eV, arises from the radiative decay of the lowest-energy excited state, related to the $^3P_0$ level of a free Bi^{3+} ion. At $T > 150$ K, the radiative decay of the thermally populated higher-energy RES, related to the $^3P_1$ level of a free Bi^{3+} ion, also takes place and the 4.19 eV emission appears. The $^1S_0 \rightarrow {}^3P_1$ electronic transitions are partly allowed due to the mixing of the triplet $^3P_1$ state with the singlet $^1P_1$ state by the spin–orbit interaction. The radiative transitions from the $^3P_0$-related state can occur due to the mixing of the $^3P_1$- and $^3P_0$-related states by the vibronic interaction with the non-totally symmetric vibrations or by the hyperfine interaction (see, e.g., [25] and references therein). As the only stable Bi isotope ^{209}Bi has a nuclear spin of $I = 9/2$, in Bi^{3+}-doped or Bi^{3+}-containing compounds with a weak vibronic interaction, mainly the hyperfine interaction can be expected to be responsible for the radiative decay of the $^3P_0$-related level. The influence of the hyperfine interaction on the probability of the radiative $^3P_0$–$^1S_0$ transitions in Bi^{3+}-doped alkali-earth oxides was considered in [6].

Hitherto, two models have been proposed for the description of the RES of the ns^2-ion-doped ionic crystals with strongly different electron–phonon and spin–orbit interactions. The systems with a *strong spin–orbit interaction and a very weak electron–phonon interaction* should be considered in the RES model, proposed by Seitz [26], which takes into account the spin–orbit interaction as the main one in the RES. In this model, the excited states of the luminescence center originate from the $^3P_0$, $^3P_1$, $^3P_2$ and $^1P_1$ levels of a free ns^2 ion which are split in the crystal field of the corresponding symmetry. For the generated energy levels, the Jahn–Teller effect is taken into account as a perturbation. The totally symmetric $^3P_0$ state is non-generated; therefore it cannot be active in the Jahn–Teller effect. The configuration coordinates (q) of the $^3P_0$ and $^1S_0$ minima in this model should coincide.

For the systems with a *strong electron–phonon interaction*, the RES theory was developed in [27]. In this theory, the interaction of impurity optical electrons with non-totally symmetric vibrations is considered as the main one in the RES, while the spin–orbit, hyperfine and other interactions are taken as small perturbations. As a result, the Jahn–Teller minima of different symmetries can be formed on the adiabatic potential energy surface of the singlet (^1P) and triplet (^3P) excited states. Due to the spin–orbit interaction, each Jahn–Teller minimum of the triplet RES is split into an upper emitting level and a lower metastable level. The applicability of this model

was confirmed by the systematic experimental study of luminescence characteristics of ns^2-ion-doped alkali halide crystals (see, e.g., the review [25]). It was also found that in the Tl^+, Pb^{2+} and Bi^{3+} centers with a strong spin–orbit interaction, each metastable minimum of the triplet RES can lie not exactly under the corresponding emitting minimum, like in the Ga^+, In^+, Ge^{2+} and Sn^{2+} centers with a weak spin–orbit interaction, but it can be shifted towards smaller configuration coordinate (q) values with respect to the emitting minimum. Due to that, the energy barriers for the thermally stimulated transitions between the metastable minima of various orientations can be much lower than those between various emitting minima (see, e.g., [13, 25, 28] and the references therein).

A free Bi^{3+} ion is characterized by the largest spin–orbit interaction energy (ξ) among all ns^2 ions ($\xi = 1.074$ eV [12]). The luminescence characteristics of two Bi^{3+}-doped crystals with strongly different electron–phonon interaction (KCl:Bi and CaO:Bi) were compared in [13]. It was concluded that the theoretical model [27] is still valid in the case of KCl:Bi but it is not valid in the case of CaO:Bi due to a very weak electron–phonon interaction in the latter system. The values of the FWHM and Stokes shift of the UV emission band indicate that the Bi^{3+} center in LuAG can be characterized by a relatively weak electron–phonon interaction and considered as an intermediate case between Bi^{3+}-doped CaO and KCl. In view of these circumstances and the experimental data obtained in this paper, a schematic configuration coordinate diagram of the triplet excited state of LuAG:Bi is presented in figure 8. A large spin–orbit splitting energy results in the appearance in the steady-state emission spectra of two separate emission components, arising from the radiative decay of the metastable and the emitting triplet RES minima. The excitation in the A absorption band results in the electronic transitions into the $^3P_1$ state. A very small light sum of the fast component in the decay kinetics of the UV emission of LuAG:Bi means that the initial population of the $^3P_1$-related relaxed excited state is comparatively small. It points to the population of the metastable $^3P_0$-related minimum mainly from the nonrelaxed $^3P_1$ state. Similar features were observed in many other Bi^{3+}-doped oxide-based materials (see, e.g., [4, 5, 8, 13, 14]). The same effect was detected also in the In^+- and Sn^{2+}-doped alkali halides and explained by the peculiarities of vibrational relaxation processes in the triplet excited state of the impurity ions [25]. In the systems with a weak electron–phonon interaction, this effect can be caused by a suitable mutual location of the corresponding adiabatic potential energy surfaces (e.g. by the intersection of the $^3P_1$- and $^3P_0$-related potential surfaces below the energy level where the $^1S_0 \rightarrow {}^3P_1$ transitions take place). A strong shortening of the fast component decay time (by two orders of magnitude as compared with that expected for the $^3P_1$ state of a Bi^{3+}-type center, see, e.g., [13, 14, 25]) can be caused by the fast non-radiative $^3P_1 \rightarrow {}^3P_0$ transitions. As the temperature increases, the $^3P_1$-related level of Bi^{3+} centers becomes thermally populated from the $^3P_0$-related level with an activation energy of 84 ± 2 meV which corresponds to the spin–orbit splitting energy of the triplet RES of a Bi^{3+} ion.

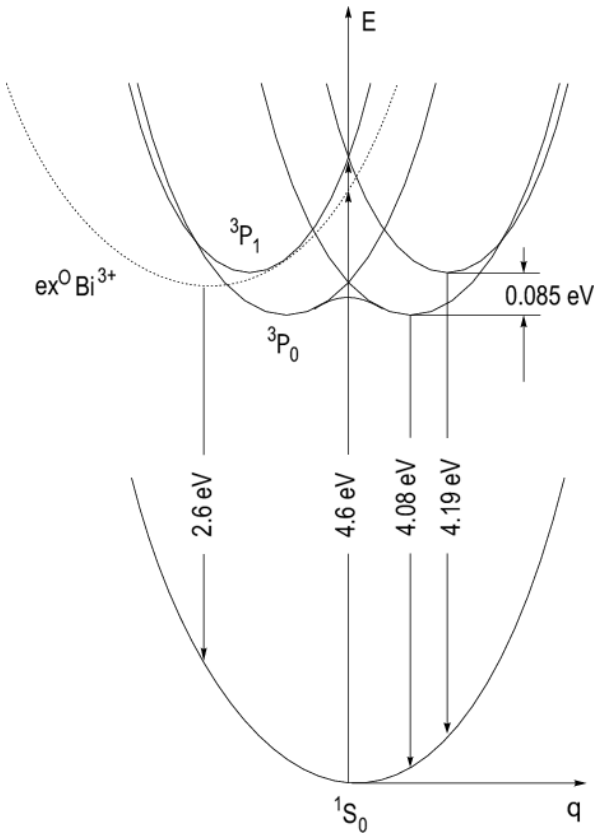

Figure 8. Schematic configuration coordinate diagram of the Bi^{3+}-related triplet excited state in LuAG:Bi. The electronic transitions between the ground state, corresponding to the $^1S_0$ level, and the excited states, corresponding to the $^3P_1$ and $^3P_0$ levels of a free Bi^{3+} ion, as well as the state of the exciton localized near Bi^{3+} ion (ex^0Bi^{3+}), are indicated by arrows.

4.2. Visible luminescence

The origin of the vis emission in LuAG:Bi SCF (as well as in many other Bi^{3+}-doped complex oxides) is surely different from that of the UV emission. As was mentioned above, two explanations have been proposed for the vis emission in garnets. In [15–17], this emission was ascribed to Bi^{3+} pairs or clusters. In [11], it was ascribed to impurity trapped excitons.

The first explanation is based on the data reported in [15–17] that the vis/UV emission intensity ratio increases with the increasing Bi^{3+} content. This effect was explained by the transformation of single Bi^{3+} centers into Bi^{3+}-related dimers and aggregates. However, unlike Pb^{2+}-doped perovskites and garnets where the effective formation of dimer and aggregate impurity centers was explained by a strong need in the Pb^{2+} ion charge and volume compensation [22], it is difficult to explain the effective formation of Bi^{3+} dimers and/or clusters in such a system as LuAG:Bi. Therefore, the concentration of these centers should be much smaller than the concentration of single Bi^{3+} centers. However, in some samples, the vis emission is even more intense compared with the UV emission. Besides, at the increasing Bi^{3+} content, dimer Bi^{3+} centers should be created first and their number should quadratically depend on the concentration of Bi^{3+}. A further increase in the Bi^{3+} content should lead to

the transformation of dimer Bi^{3+} centers into more complex aggregates of Bi^{3+} ions. As the spectra of dimers and aggregates have to be different, an increase in the Bi^{3+} content should result in a gradual shift of the emission and excitation bands and redistribution of their intensities (similar to that observed for the LuAG:Pb ceramics in [22]). However, no shift of both the 2.6 and the 2.75 eV emission band was observed, despite the change in the Bi^{3+} content by 19 times (see also [15]). The large difference in the values of the Stokes shift and FWHM of the UV and vis emissions (about 3–4 times) was never observed for single and dimer centers (see, e.g., [7, 22, 28, 29] and references therein). The close location of the excitation spectra of the UV and 2.6 eV emissions and the redistribution of their intensities indicate that both these emission bands are most probably connected with the same center. The peculiarities of the decay kinetics of the vis emissions also indicate that the vis emission bands of LuAG:Bi cannot arise from dimer Bi^{3+} centers.

We assume that the 2.6 eV emission of LuAG:Bi arises from the radiative decay of an exciton localized near a Bi^{3+} ion (see also [11]). A similar interpretation was proposed for the well-known visible luminescence of a CsI:Tl scintillator [30, 31] and also of some other Tl^{+}- and Pb^{2+}-doped cesium halides (see, e.g., [31–34] and references therein), as well as for Pb^{2+}-doped $CdCl_2$ crystals [35]. Indeed, the large values of the Stokes shifts and FWHM, as well as the low-temperature luminescence decay kinetics, namely relatively short ($\sim 10^{-5}$ s) decay times at 4.2 K and especially their temperature dependences, pointing to a very small ($\sim 10^{-4}$ eV) spin–orbit splitting energy of the triplet RES as compared with that in a Bi^{3+} ion ($\sim 10^{-1}$ eV), are also characteristic for the radiative decay of the triplet exciton state. Two decay components of this emission, 26 and 72 μs, can arise from the radiative decay of the upper and the lower emitting levels of the triplet relaxed excited state, respectively, located about 0.19 meV above the metastable level of this state. Thermally stimulated transitions between the metastable and emitting levels explain the changes in the τ values at $T < 15$ K. A faster shortening of the decay times in the temperature range of 25–100 K can be explained by the thermal population of the singlet state of the localized exciton from the triplet state. In this case, the energy distance between the triplet and singlet exciton levels is 4.7 ± 0.5 meV.

The processes of the localized exciton states creation under excitation in the impurity-induced absorption bands have been considered in detail for CsI:Tl [32] and CsI:Pb [33] crystals. It was suggested that, under excitation in the impurity-induced absorption bands, an electron transfer occurs from a halogen ion to an impurity ion, resulting in the creation of an electron impurity center and a self-trapped hole. A fast tunneling recombination in the close pairs of the optically created electron and hole centers results in the appearance of the localized exciton emission (see also [36]). In LuAG:Bi, the localized exciton states can also be produced as a result of photostimulated electron transfer processes (see, e.g., [3]). As a result, the electron Bi^{2+} and hole Bi^{4+} or O^{-} centers can be created. The formation of Bi^{2+} and Bi^{4+} ions is possible due to a variable valence of a Bi ion [23]. The possibility of formation of Bi-related hole centers was mentioned in [11]. The trapping of holes at O^{2-} ions in LuAG, resulting in the formation of O^{-} centers, was detected by the ESR method in [37]. The subsequent immediate electron–hole recombination close to the Bi^{3+} ion results in the formation of an exciton localized near the Bi^{3+} ion. A small (0.03 eV, see table 1) shift of the excitation band of the vis emissions with respect to that of the UV emission can be explained by the mutual location of the corresponding nonrelaxed levels and different relaxation ways into the corresponding excited states minima (figure 8). Note that, in CsI:Tl, the excitation band of the Tl^{+}-related localized exciton emission is also slightly shifted with respect to the A band in the excitation spectra of the A_T and A_X emission bands of Tl^{+} centers [31]. Like in CsI:Tl [31], thermally stimulated transitions take place between the states, responsible for the UV and 2.6 eV emission bands of LuAG:Bi, which indicate that both these bands arise from the same Bi^{3+} center.

The large Stokes shift and FWHM of the 2.75 eV emission and especially the similarity of its decay kinetics to that of the 2.6 eV emission indicates that this emission is also of an exciton origin. Indeed, the decay time of this emission at 4.2 K is 40 μs, the energy distance between the emitting and the metastable minimum is 0.11 meV and between the singlet and triplet exciton states, about 2.7 meV. The increase of the vis/UV emission intensity ratio accompanied by the higher-energy shift of the vis emission band observed in [17] allows us to assume that the 2.75 eV emission arises from an exciton localized near a dimer Bi^{3+} center.

5. Conclusions

The coexistence of the Bi^{3+}-ion-related energy levels and the levels of an exciton, localized near the Bi^{3+} ion, is found in the triplet relaxed excited state of the luminescence center in LuAG:Bi. The radiative decay of the emitting and metastable minima, arising from the $^3P_1$- and $^3P_0$-related levels of a free Bi^{3+} ion, results in the appearance of UV emission. The radiative decay of an exciton, localized near the single Bi^{3+} ion, results in the appearance of the lower-energy vis emission band. The weak higher-energy vis emission band, showing a stronger intensity dependence on the Bi^{3+} content, is assumed to arise from an exciton localized near a dimer Bi^{3+} center. The structure and the parameters of the triplet RES of the Bi^{3+} center and of the state of the excitons localized near single and dimer Bi^{3+} centers are determined.

A similar excited state structure can be characteristic for Bi^{3+}-related centers in some other rare-earth garnets and perovskites.

Acknowledgments

This work was partly supported by the Estonian Science Foundation project no. 7507, the project of the Czech Science Foundation no. 202/08/0893, the project of the Ukrainian Ministry of Education and Science no. SF-28 F and by the EC Research Infrastructure Action under FP6 ‘Structuring the European Research Area’ Programme (‘Integrating Activity on Synchrotron and Free Electron Laser Science’). The authors are indebted to Acad. V. Hizhnyakov for valuable discussions.

References

[1] Lushchik Ch B, Lushchik N E and Muuga I A 1963 *Tr. Inst. Fiz. Astron. Akad. Nauk. Est. SSR* **23** 22
[2] Zazubovich S, Lushchik N E and Lushchik Ch B 1963 *Sov. Phys.—Opt. Spectrosc.* **15** 381
[3] Lacklison D E, Scott G B and Page J L 1974 *Solid State Commun.* **14** 861
[4] Hughes A E and Pells G P 1975 *Phys. Status Solidi* b **71** 707
[5] Ellervee A F 1977 *Phys. Status Solidi* b **82** 91
[6] Zavt G S and Ellervee A F 1979 *Phys. Status Solidi* b **94** 757
[7] Wolfert A and Blasse G 1985 *J. Solid State Chem.* **59** 133
[8] Wolfert A and Blasse G 1985 *J. Lumin.* **33** 213
[9] Boulon G 1987 *Spectroscopy of Solid-State Laser-Type Material* ed B Di Bartolo (New York: Plenum) p 223
[10] Blasse G 1988 *Prog. Solid State Chem.* **18** 79
[11] Ilmer M, Grabmaier B C and Blasse G 1994 *Chem. Mater.* **6** 204
[12] Kang J G, Yoon H M, Chun G M, Kim Y D and Tsuboi T 1994 *J. Phys.: Condens. Matter* **6** 2101
[13] Aceves R, Barboza Flores M, Maaroos A, Nagirnyi V, Perez Salas R, Tsuboi T, Zazubovich S and Zepelin V 1996 *Phys. Status Solidi* b **194** 619
[14] Nikl M, Novoselov A, Mihokova E, Polak K, Dusek M, McClune B, Yoshikawa A and Fukuda T 2005 *J. Phys.: Condens. Matter* **17** 3367
[15] Setlur A A and Srivastava A M 2006 *Opt. Mater.* **29** 410
[16] Zorenko Yu, Gorbenko V, Voznyak T, Vistovsky V, Nedilko S and Nikl M 2007 *Radiat. Meas.* **42** 882
[17] Zorenko Yu, Mares J A, Kucerkova R, Gorbenko V, Savchun V, Voznyak T, Nikl M, Beitlerova A and Jurek K 2009 *J. Phys. D: Appl. Phys.* **42** 075501
[18] Donker H, Yamashita N, Smit W M A and Blasse G 1989 *Phys. Status Solidi* b **156** 537
[19] Suzuki Y, Sakuma T and Hirai M 1997 *Mater. Sci. Forum* **239–241** 219
[20] Fischer P, Haelg W, Stoll E and Segmueller A 1966 *Acta Crystallogr.* **21** 765
[21] Weber M J 2003 *Handbook of Optical Materials* (Boca Raton, FL: CRC Press)
[22] Babin V, Bichevin V, Gorbenko V, Makhov A, Mihokova E, Nikl M, Vedda A, Zazubovich S and Zorenko Yu 2009 *Phys. Status Solidi* b **246** 1318
[23] Eucken A (ed) 1950 *Zahlenwerte und Funktionen, I. Band, Atom- und Molekularphysik, I Teil, Atome und Ionen* (Berlin: Springer) p 439
[24] Lushchik N E and Lushchik Ch B 1960 *Sov. Phys.—Opt. Spectrosc.* **8** 839
[25] Zazubovich S 1994 *Int. J. Mod. Phys.* B **8** 985
[26] Seitz F 1938 *J. Chem. Phys.* **6** 150
[27] Hizhnyakov V V and Kristoffel N N 1984 *The Dynamical Jahn–Teller Effect in Localized Systems* ed Yu Perlin and M Wagner (Amsterdam: Elsevier) p 383
[28] Nagirnyi V, Soovik T, Vaino P, Zazubovich S and Jaanson N 1991 *Phys. Status Solidi* b **164** 493
[29] Tsuboi T and Jacobs P W M 1991 *J. Phys. Chem. Solids* **52** 69
[30] Nagirnyi V, Zazubovich S, Zepelin V, Nikl M and Pazzi G P 1994 *Chem. Phys. Lett.* **227** 533
[31] Nagirnyi V, Stolovich A, Zazubovich S, Zepelin V, Mihokova E, Nikl M, Pazzi G P and Salvini L 1995 *J. Phys.: Condens. Matter* **7** 3637
[32] Babin V, Kalder K, Krasnikov A and Zazubovich S 2002 *J. Lumin.* **96** 75
[33] Babin V, Kalder K, Krasnikov A, Nikl M, Nitsch K and Zazubovich S 2002 *Phys. Status Solidi* b **234** 689
[34] Babin V, Krasnikov A, Nikl M, Nitsch K, Stolovich A and Zazubovich S 2003 *J. Lumin.* **101** 219
[35] Moine B, Pedrini C and Ghiordanescu V 1994 *J. Phys.: Condens. Matter* **6** 4093
[36] Fu C-R, Chen L-F and Song K S 1999 *J. Phys.: Condens. Matter* **11** 5517
[37] Nikl M, Laguta V V and Vedda A 2008 *Phys. Status Solidi* b **245** 1701